CNIC-00637
ASIPP-0033

中国核科技报告

CHINA NUCLEAR SCIENCE & TECHNOLOGY REPORT

HT-6B托卡马克杂质输运

THE IMPURITY TRANSPORT IN HT-6B TOKAMAK

原子能出版社

中国核情报中心
China Nuclear Information Centre

黄荣：中国科学院等离子体物理研究所助理研究员，1983年毕业于安徽大学物理系，1991年获等离子体物理研究所博士学位。

Huang Rong: Researcher of Institute of Plasma Physics, Academia Sinica. Graduated from Physics Department of Anhui University in 1983 and got Ph. D. degree at Institute of Plasma Physics Academia Sinica in 1991.

CNIC-00637
ASIPP-0033

HT-6B 托卡马克杂质输运

黄 荣　谢纪康　李林忠　何也熙
汪舒娅　邓传宝　李国相　邱励俭

（中科院等离子体所，合肥）

摘　要

在 HT-6B 托卡马克上，通过测量杂质的真空紫外线辐射和可见线辐射，得出杂质各电离态的稳态空间分布。建立了杂质输运计算程序，模拟分析出该装置上杂质输运系数和其它与之有关的参数。通过对慢磁压缩下杂质线辐射时空分布的测量和模拟分析，得出了杂质约束因磁压缩而增强、杂质再循环随之降低等结论。同时对该装置上杂质输运特征进行了分析与讨论。

THE IMPURITY TRANSPORT IN HT-6B TOKAMAK

Huang Rong Xie Jikang Li Linzhong He Yexi
Wang Shuya Deng Chuanbao Li Guoxiang Qiu Lijian
(INSTITUTE OF PLASMA PHYSICS,
ACADEMIA SINICA, HEIFEI)

ABSTRACT

The quasi-stationary profiles of the impurity ionization stages in HT-6B tokamak were determined by monitoring the VUV (vacuum ultraviolet) and visible line emissions from impurities. An impurity transport code was set up. The impurity transport coefficients and other parameters of impurities in that device were simulated and determined. From the measurement of impurity emission profiles and simulation analysis, it was concluded that the impurity confinement was improved and the impurity recycling was reduced by the slow magnetic compression. Some characteristics of impurity transport in that device were also discussed.

INTRODUCTION

It has been known that the tokamak plasma parameters and the energy confinement time may be reduced by plasma impurity radiation. The plasma MHD stabilities may also be influenced by the impurities in it. In some H-mode discharges and other kinds of improved confinement discharges, it is often happened that the impurity accumulation is very serious and uncontrollable, which is not tolerable for future reactors. The impurity accumulation in tokamaks is not only determined by the impurity influx from the edge, but also the impurity transport in plasma. The impurity anomalous transport in tokamak has not been clearly explained yet and it is one of the main subjects for fusion plasma research. It's important to determine the impurity transport coefficients and their changes for different kind of discharges in tokamaks.

In HT-6B tokamak, some ionization stage profiles of oxygen and carbon impurities were determined with a grazing incident VUV monochrometer and a multichannel visible spectrometer. A one-dimensional impurtiy transport code was set up. Some characteristics of the impurity transport have been analysed. It was concluded from the changes of the impurity stage profiles that the impurity confinement was improved and the impurity recycling was reduced by the slow magnetic compression along minor radius. The detailed explanation of the profile changes is also an important information for the slow magnetic compression.

1 THE ABSOLUTE SPECTROSCOPIC MEASUREMENT OF THE IMPURITIES

It has been known from the spectrum photographed by many shots on HT-6B tokamak that the main components of impurities in the plosma are oxygen and carbon[1]. The spectroscopic instruments for impurity line emission monitoring in this device included a grazing incident VUV monochrometer and a multichannel visible spectrometer. The VUV line emission profile were determined shot-by-shot by adjusting a gold evaporated mirror in front of the VUV spectrometer, and this method was miainly used for the resonant lines of OV, OVI, CIV, and so on. On the other hand, the profiles of visible (or near ultraviolet) emissions from the impurity low stages can be determined in one shot by the multichannel visible spectrometer, with a two-lens image system in front of its entrance and a multichannel

optical fiber attached to its exit slit, and it's mainly used for the monitoring of O Ⅱ ~O Ⅳ and C Ⅲ. All the detectors are photomultipliers. The visible spectrometer has been absolutely calibrated with a standard lamp, and the VUV spectrometer has been absolutely calibrated by the branching-ratio method. The parameters about the measured line are shown in Table 1 and Table 2 (taking from reference [2]). the measured visible lines here are all the bright and easily distinguished visible lines according to the photographed spectra in this device.

Table 1 The monitored VUV lines

stage	λ(10 ^{10}m)	multiplet	configuration	E_{ij}(eV)
O Ⅵ	1032	$2S-{}^2P^o$	2s−2p	12.0
O Ⅴ	630	$1S-{}^1P^o$	$2s^2-2s2p$	19.7
O Ⅳ	790	$2P^o-{}^2D$	$2s^22p-2s2p^2$	15.7
O Ⅱ	835	$2P-{}^3D^o$	$2s^22p^2-2s^22p^3$	14.9
C Ⅳ	1548	$2S-{}^2P^o$	2s−2p	8.0

The major parameters of the small tokamak HT-6B are as following: major radius $R=45$ cm, minor radius $a=12.5$cm, plasma current $I_p=20\sim40$ kA, toroidal field $B_t=0.5\sim0.8$ T, line average electron density $n_e=0.4\times10^{13}\sim2.0\times10^{13}$cm^{-3}, discharge duration is about 20 ms. The quasi-steady-state plasma is arrived at $T=6$ ms. For the ordinary parmeters: $I_p\sim25$kA, $n_e\sim1.1\times10^{13}$cm^{-3}, $B_t\sim0.7$ T, the radiation profiles of O Ⅱ ~O Ⅵ determined with the VUV monochrometer and the visible spectrometer are shown in Fig. 1. The profile of C Ⅳ was also determined as in Fig. 2. With the measured results, it is possible for us to make transport analyses for these impurities in the next section.

Table. 2 The monitored visible lines

stage	ground	λ(Å)	configuration	terms	E_{ij}(eV)	Transition from upper to ground
O Ⅱ	$2s^22p^3(^4S^o)$	4416	$2p^23s-2p^23p$	$^2P-{}^2D^o$	26.3	spin exchange
O Ⅱ	$2s^22p^3(^3P)$	3759	2p3s−2p3p	$^3P^o-{}^3D$	36.5	no*
O Ⅳ	$2s^22p(^2P^o)$	3737	$2s2p3p-2s2p3d$	$^4D-{}^4F^o$	61.4	spin exchange

* "no" means there are no dipole, quadrupole and spin exchange transition.

2 THE NUMERICAL ANALYSIS OF IMPURITY TRANSPORT

The stage profiles of a given impurity in tokamak plasma are determined by the transport and the electron-impurity collision ionizations and recombinations. They can be numerically modelled through a set of coupled continuity equations in cylindrical coordinate as following:

$$\partial n_z/\partial t = -1/r[\partial(r\Gamma_z)/\partial r] + n_e[n_{z-1}S_{z-1} - n_z S_z + n_{z+1}\alpha_{z+1} - n_z\alpha_z]$$
$$Z = 1, \cdots, Z_N \tag{2.1}$$

In Which, n_z is the density of the z-th stage of the impurity, Z_N is the nuclear charge, S_z, α_z are the total ionizition and recombination rate coefficieants, Γ_z is the transport flux along minor radius which is driven by the impurity diffusion and convection effects[3], i. e.

$$\Gamma_z = -D(r) \cdot \partial n_z/\partial r - V \cdot f(r) n_z \tag{2.2}$$

Up to now, $D(r)$ and $f(r)$ can only be determined from experiment results because of the anomalous transport effect, and it's generally assumed that D and V are independent of stages and radial position, and the $f(r)$ is given with the following from[3]:

$$f(r) = r/a \tag{2.3}$$

in which, a is the plasma radius. With this form of $f(r)$, the total impurity density distribution in a tokamak will be in the Gaussian form for the source and sink free region. There is also an another form of $f(r)$ that is ofter used in order to relate the total impurity density profile to the electron density profile[4]:

$$f(r) = \partial[\ln(n_e(r))]/\partial r \tag{2.4}$$

Here, with Eq. (3.1), (3.2), (3.3) and the boundary condition:

$$\begin{cases} \partial n_z/\partial r|_{r=0} = 0 \\ n_z(a) = 0 \end{cases} \tag{2.5}$$

we edit a one dimensional impurity transport code. The impurity atom profile is given by the results from a slab model[5]:

$$n_0(r) = n_0(a) \cdot \exp[-1/V_0 \int_r^a S_0(r) \cdot n_e(r) dr] \tag{2.6}$$

The ionization rate coefficients are given by the Lotz semi-empirical formula. But in this paper, for the stages lower than O^{+5} the Lotz coefficients are multiplied by 0.5 according to reference [6]. The recombination rate coefficients are given by Kramer formula (radiative recombination) and Burgess formula (de-electronating recombination). The relation between the stage densities and the spectral line em-

mission intensities are given by the solar corona model. The excitation coefficients from grounds to the upper states of all the resonant lines and some visible lines can be given by the formula from the Coulomb-Born approximation or the formula from the Coulomb-Bethe approximation. However for the upper state of the O Ⅱ visible line we have monitored, as for as we know, there is no any simple formula that can give the exciting coefficient from the fround, since neither a dipole-allowed transition nor a forbidden monopole or quadrupole transition, nor a spin-exchange transition is existed from the upper state to the ground. But from the results of HT-6B spectroscopic experiment and our modelling, it has been found that the equivalent exciting rate coefficient for the monitored O Ⅱ state in this paper is approximatly equal to 1/5 of the exciting coefficient for the upper stages with the same principal quantum number n but having a quadrupole forbidden transition to ground state.

According to the experiment results from a variety of the diagnostics such as Thomson scattering, SX emission, electromagnetic diagnoses (I_P, V_P) and ECE emission, the central electron temperature $T_e(0)$ for HT-6B in the closest discharge region is within 130～200 eV, and for the discharge parameters corresponding to the profile measurement of Fig. 1 and Fig. 2, the $T_e(0)$ is about 170 eV. From the SX profiles, the T_e profile here can be approximately given as:

$$T_e(r)=160(1-r^2/a^2)^{1.5}+10 \qquad eV \tag{2.7}$$

On the other hand, from the measurement of the line average density, we assume the electron density profile as:

$$n_e(r)=1.5\times10^{13}(1-r^2/a^2)+1.0\times10^{12} \qquad cm^{-3} \tag{2.8}$$

Within these plasma parameters, the experiment results of oxygen stage profiles (Fig. 1) can be numerically simulated approximately both in profiles and in absolute intensities with the transport coefficcients $D=2.5\times10^4$ cm^2s^{-1} and $V=5.0\times10^3$ $cm\cdot s^{-1}$, as shown in Fig. 3. It means that the impurity transport process in HT-6B can be empirically described with these transport coefficients. It can be also shown by the numerical modelling that the impurity confinement time $\tau_e=2.0$ ms and the average effective ionic charge $Z_{eff}=1.5$. The resonant line emission of CIV has been also numerically simulated (Fig. 2) and the results shown that carbon impurity transport in HT-6B can also be described with the similar coefficents as oxygen. It can be also concluded from these modelling that the total density of corbon ions is about 30% of that of oxygen. the average effective ionic charge Z_{eff} is about 1.6 by the total contribution of oxygen and carbon.

It has been found from the simulation that the majority of oxygen and carbon impurities in HT-6B tokamak is the He-like ions (Fig. 4). In the plasma columu center, the densities of oxygen and carbon He-like ions reach separately 80% and 70% of the total density of their own element. But up to now in HT-6B, the line emission of OⅦ or CV has not been clearly found using the VUV monochrometer because of the partcularity of the He-like ion configuration. For example, the resonant exciting energy of OⅦ is higher than 560 eV, which is much greater than the resonant exciting energy of OⅥ or other lower stage ions. With the electron temperatures in HT-6B, the exciting coefficients of the main exciting levels of OⅦ are 3 or 4 orders smaller than that of OⅥ or other lower stages, and the emissivities are also 2 or 3 orders smaller. So, the emission of OⅦ is too weak to be found in HT-6B with the VUV monochrometer without particular treatment for the detector.

From the preceding statement it can be found that the electron density and the impurity confinement time in the small tokamak HT-6B is smaller than the general parameters in other tokamaks. The smaller the n_e is, the lower the ionization rate will be, and the smaller the τ_z is, the faster the impurity transport will be. These will cause the ion stage profiles in HT-6B to have the particular characteristics. The electron temperature around each stage profile peak positions of oxygen and carbon in the plasma is approximately equal to the separate ionization potential of these stages. But in most tokamaks for the lower Z impurities, these peaks occur at about one third of the ionization potential. The total line emission power profile in HT-6B therefore become flat as shown in Fig. 5, which was simulated by accumulating the major line emission power of all the oxygen stages[7]. It can be found that, when T_e is higher than 50 eV, the oxygen emission power per $n_e n_z$ with the solar corona stage equilibrium condition, which is about 10^{-27} W · cm^{-3}[8], is one order smaller than the calculated results in Fig. 5. This difference is mainly caused by the sensitive influence on exciting rate by T_e when T_e is remarkably lower than the exciting potential. The calculated total radiated power from oxygen in HT-6B quasi-steady state is about 5 kW which is equivalent to 10% of the ohmic heating power. The actually power loss by impurities in HT-6B must be higher than this value if the carbon radiation, the ionization and heating power of these impurities are considered. The lower impurity loss power in HT-6B is not only due to the lower accumulation of impurities, but also the lower plasma densities.

3 THE EFFECT OF SLOW MAGNETIC COMPRESSION ON IMPURITY TRANSPORT

The characteristics of the slow magnetic compression along minor radius in HT-6B tokamak is the toroidal feild rise time (about 2. 5ms) longer than the energy confinement time (about 0. 5～1. 0ms). Generally, after the plasma current has reached to the statioanary state, the B_t will rise from 0. 42 T to 0. 64～0. 72 T and maintain has reached there. The experiment results showed that the plasma energy confinement time was improved and the plasma parameters were increased by the compression[9]. It will also be shown from the following analysis of the impurity emissions that the impurity confinement was also improved with the slow magnetic compression.

The multichannel SX emission signals, which could describe the compression effect most obviously, show that the plasma parmeters rise within $r<6.0$ cm and fall down for $r>6.0$ cm by compression (Fig. 6). The further analysis concluded that the central electron temperature and density would be increased by 20% and 10% separately after compression[10].

The changes of the O Ⅱ, O Ⅲ, O Ⅳ emission profiles induced by compression are shown in Fig. 7. It shows that when B_t increased, the emissivity in plasma edge decreased because of the decrease of edge plasma parameters, and the profiles shift slightly towards center. After compression, the profile positions moved back and lay even more out than that before compression, with slighly decrease of the peak intensities. The changes of O Ⅴ and O Ⅵ V U V line emission profiles by compression are shown in Fig. 8. Their emmission intensities at plasma edge haven't any obvious changes in all the compression period, but the profile peak positions move outward considerably and the peak emissivities have a lot of decrease after compression.

With the spectroscopic phenomena described above, the changes of the impurity transport by compression can be numerically analysed. First, it can be verified that only with the changes of the plasma parameters we can't explain the changes of the impurity profiles in Fig. 8. With impurity transport code, the O Ⅴ and O Ⅵ emission profiles before compression are modelled as shown with the solid lines in Fig. 9. The emission profiles, which are wished to represent the profiles after compression are also simulated, with 20% increased $T_e(0)$ and 10% increased $n_e(0)$,

but without changes of the T_e and n_e for $r>6.0$ cm and without changes of the impurity transport coeficients, are shown with dotted lines in Fig. 9. It can be seen in Fig. 9 that the simulated changes of these profiles before and after compression are too small to explain the experiment results, although the later do move slightly outward. These differences would be even more smaller if we take the plasma parameters for $r>6.0$ cm slightly decreased after compression as it happened in experiments. Although the plasma parameter profiles and their changes after compression given here is not accurate, the conclusion is very definite that the influence on impurity stage profiles caused by the changes of the background plasma parameters by compression is too little to match the experiment results. The changes of the impurity transport coefficients must be considered in the numerical anlysis to explain the experiment. The dash lines in Fig. 9 that satisfy the experiment results best are just obtained by decreasing the impurity diffusion coefficient from 2.5×10^4 to 1.8×10^4 cm$^2\cdot$s^{-1} and convection coefficient from 5.0×10^3 to 3.6×10^3 cm$\cdot$s^{-1}, and also decreasing the impurity influx at plasma edge with the changed plasma parameters by compression. It means that the impurity confinement is improved by the slow magnetic compression. From the numerical results, the impurity confinement time is increased from 2.0 ms to 2.8 ms and influx from edge is decreased by 30%.

Actually, the improvement of the impurity confinement can be qualitatively illustrated from the changes of the O Ⅱ, O Ⅲ and O Ⅳ line profiles shown in Fig. 7. If there are no changes of impurity transport, the decrease of the plasma parameters in $r>6.0$ cm region can only cause the O Ⅱ, O Ⅲ and O Ⅳ profiles, which mainly exist in $r>6.0$ cm region, to move inward that contradicts with the outward movement in experiment. So, the changes of the impurity transport must be happened in this period. Only the increase of impurity confinement can cause these profiles to move outward.

In the compression, the changes of the different stage profiles also have the following characteristics: During the period of compression (i. e. when B_t is rising), the emissivity of lower stages (such as O Ⅱ, O Ⅲ) at plasma edge decrease remarkably, but for higher stages (such as O Ⅴ, O Ⅵ), no such changes take place; on the other hand, after compression (i. e. when B_t arrives at a high value and maintains there), the outward movement and the decrease of the emissivity of O Ⅴ and O Ⅵ profile peaks are greater than those of the lower stages. By the nu-

merical simulation it can be seen that this phenomena is due to the natures of the impurity transport and the plasma parameter profiles in HT-6B. The numerical result of the stationary transport fluxes of different stages are shown in Fig. 10, from which it can be seen that the fluxes of O^{+4} and O^{+5} are much greater than that of the lower stages in $r<a/2$ region. Sc, the emissivity of O Ⅴ and O Ⅵ in $r>a/2$ region not only depends on the ionization of lower stages, but also the outward impurity transport from the centre. However, for the lower stages in $r>a/2$ region, the only source is the ionization process, so the edge emissivities of the lower stages, such as O Ⅰ and O Ⅱ, markedly decrease, and their profiles appear swing inward because of the decrease of the edge plasma parameters just during compression. On the other hand, because the n_e and T_e profiles in $r>a/2$ region are steeper than in the inner region, if the impurity transport coefficients are changed, the movement of O Ⅴ and O Ⅵ profile peaks must be greater than that of O Ⅰ, O Ⅱ and O Ⅳ.

It has also been noticed from the Langmuir probe signals that the edge plasma parameters can be decraesed to the half in a long period (about 6～8 ms) after compression. It may be the decrease edge parameters that cause the reduction of the impurity influx from edge. The increase of the impurity confinement must be related to the changes of plasma parmeters or the increase of the toroidal field. But the direct physical process causing the decrease of the anomalous transport in HT-6B compression experiment can't be defined in this paper.

It has also be noticed that, the influence on the confinement of main particles (H^+) by compression is different from impurities. The space multichannel H_α emissions for plasma compression are shown in Fig. 11. During compression (i. e. for the B_t rise period), all the H_α signals decreased, especially for the emission from edge, and it means that the edge plasma parameters markedly reduced and the particle confinement was somewhat improved. But all the H_α signals nearly went back to the original intensities after compression. For there is no obvious changes of line average density during this whole period, that means the main particle confinement has not improved so obviously as impurities after the slower magnetic compression.

4 DISCUSSIONS

Among the tokamak impurity spontaneous emissions, ganerally only the resonant emissions are used for the impurity transport analysis because of the lower ex-

citing energy, stronger line intensities, less dependence on T_e for most of the case and the more accurate atom coefficients of the resonant emmissions. But in HT-6B tokamak, the profile peaks of the stages occur at radial positions where the electron temperatures are approximately equal to their ionization potentials. For the majority particles of oxygen lower stages, the upper levels of the monitored visible lines can be highly excited, the emissivities may be very intense and only be slightly affected by the uncertainty of the electron temperature profiles there. So it is very convenient to utilize the visible (or ultraviolet) lines to study the distribution and transport of impurities in HT-6B.

The uncertainty that most probably introduced into in the impurity transport anlysis may come from the uncertainty of the atomic process coefficients. By transport analysis, we can reach the conelusion that the impurity profiles in HT-6B are mainly determined by the processes of transport and electron collision ionization and very slightly affected by the effect of recombination, then it may be inferred from Eq. (2.1) and (2.2) that the uncertainty of the numerical result of transport coefficients can't exceed the maximum of the ionization coefficient uncertainties, which are generally considered with a factor of two confidence.

Although HT-6B is a small tokamak and the plasma parameters are lower, the charge exchange recombination hasn't been included in the numerical calculation. The central neutral hydrogen atom density determined from the resonant fluorescence of H_α is generally about $1.1\times10^{8}\,cm^{-3}$ when the line average electron density is about $1.0\times10^{13}cm^{-3}$. Even for low electron density discharges ($n_e=0.4\times10^{13}$), the $n_0(0)$ is generally smaller than $8\times10^{8}cm^{-3}$[11]. It has been verified in reference [12] that in the low collision energy region the charge exchange recombination cross sections from the PSS (Perturbed-stationary-state) theoretic approximation matches the experiment results best, and the results from other theory approximation are much larger. It is deduced with the PSS results that the charge exchange recombination rates of the majority stages in the main region of HT-6B plasma are smaller than their dielectronic recombination rates. Actually, even if some stages' charge exchange recombination rates is slightly greater than their dielectronic recombination rates, they can also be neglected as long as they are still smaller than the rates of impurity ionization and transport. If there is a speciall attention to the plasam boundary where the n_0 may be very high and plasma parameters are very low, it may be needed to consider the charge exchange recombination

process.

The uncertainties of the HT-6B plasma parameters $n_e(r)$ and $T_e(r)$, especially T_e, are also important factors for the uncertainties of numerical results of impurity transport analyses. In order to investigate this effect, two sets of numerical results of O V and O VI profiles are shown in Fig. 12, with the same transport coefficients but nearly 20% difference of electron temperature exists every where. The profile shapes and peak positions are very similar. It can also be seen from Fig. 9 that the two sets of the O V and O VI profiles, only with different $n_e(r)$ and $T_e(r)$ profiles caused by compression, are very similler both in profile and absolute value. All of these demonstrate that the basic conclusion of this paper can't be affected seriously by the uncertainties of HT-6B $n_e(r)$ and $T_e(r)$ profiles.

The characteristics of HT-6B tokamak impurity transport described in this paper will be helpful for the further plasma experiment researches in this small device, in which some parameters about impurities may be very different from that in larger devices. The conclusion that the slow maganetic compression along minor radius improve the impurity confinement is not only a compatible result with the improvement of energy confinement, but also a clue for us to make a further reseach of the impurity anomalous transport.

ACKNOWLEDGEMENT

We gratefuly acknowledge the HT-6B group for the help over all the experiments on the device and Ms. Zhang Cheng for her kindly help.

REFERENCES

[1] Wei Lehan, Fu Jikai, Wang Shuya. ACTA Optica Sinica, 1984,4:84

[2] Wiese, W L et al., Atomic Transition Probablities NSRDS-NBS 4. Washington: D. C. 1966

[3] Isler, R C Nucl. Fusion. 1984, 24: 1599

[4] Stratton, B C et al., Nucl. Fusion. 1989, 29: 437

[5] Zhang Cheng, Nucl. Fusion and Plasma Phys. 1987, 7: 42 (in chinese)

[6] TFR Group, Nucl. Fusion 1982, 22: 1173

[7] Huang Rong, et al. Nucl. Fusion and Plasma Phys. 1992,12: 41

[8] C. Breton, et al. Nucl. Fusion, 1976, 16: 891

[9] Xie Jikang, HT-6B Group, IAEA-CN/53-A-6
[10] He Yexi, et al. ASIPP/77, 1989
[11] Mao jiansan, et al. Power Laser and Particle Beam. 1990, 2: 67 (in chinese)
[12] R. A. Phaneuf, et al. Phys. Rev. A. 1982, 26: 1892

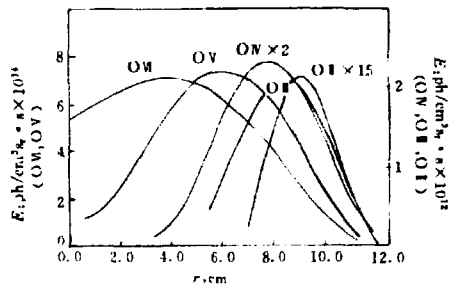

Fig. 1 The experiment results of O Ⅱ, O Ⅲ, O Ⅳ, O Ⅴ and O Ⅵ profiles. O Ⅴ and O Ⅵ were determined with V U V monochrometer and O Ⅲ and O Ⅳ with visible monochrometer.

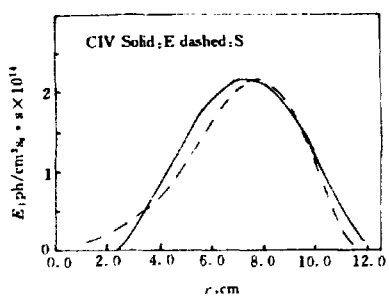

Fig. 2 The experiment result (solid line) and simulated result (dash line) of C Ⅳ profile

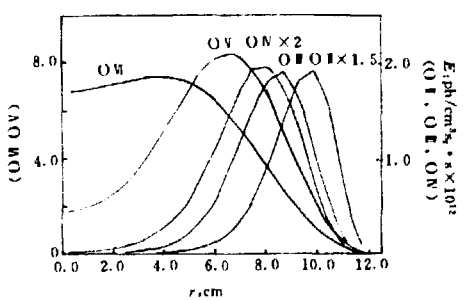

Fig. 3 The simulated results of O Ⅰ ~O Ⅵ profiles with $D=2.5\times10^{4}cm^{2}/s$, $V=5.0\times10^{3}cm/s$.

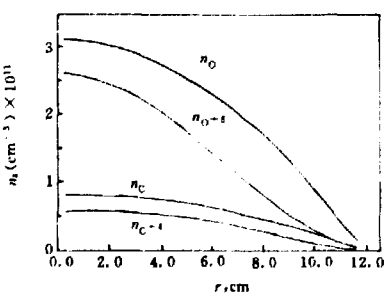

Fig. 4 The simulated results of the density profiles of O^{+6}, C^{+4}, the total oxygen density (n_{O_t}) profile and the total carbon density (n_{C_t}) profile.

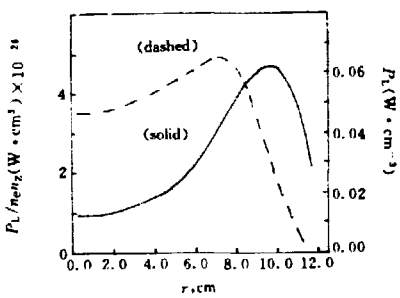

Fig. 5 The numerical results of oxygen radiated power loss profiles: P_1 and $P_1/n_e'n_z$.

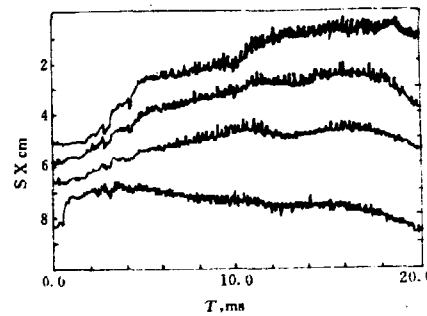

Fig. 6 The SX signals (from the top: $r=2.0$, 4.0, 6.0, 8.0 cm) in magnetic compression. B_t begins to rise at $t=10.0$ ms and arrives high plateau at about $t=12.5$ ms.

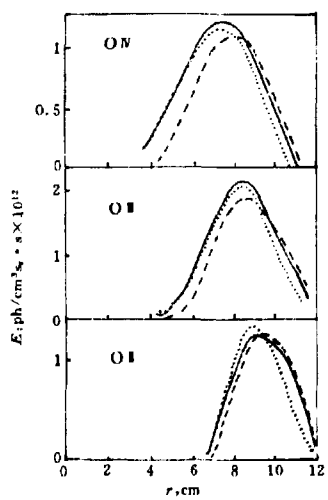

Fig. 7 The experiment results of O Ⅰ, O Ⅱ and O Ⅳ profiles before compression (solid lines), during compression (dotted lines) and after compression (dashed lines), which were determined with visible spectrometer.

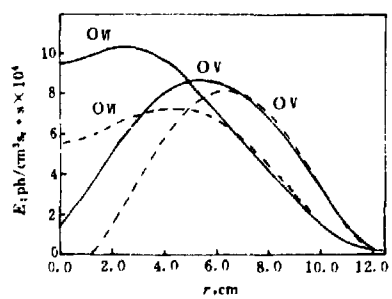

Fig. 8 The peak positions of O Ⅴ and O Ⅵ profiles moved outward very obviously after compression. Solid line: before compression; dashed line: after compression.

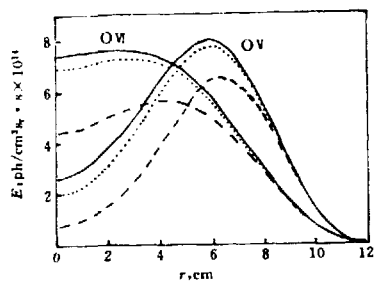

Fig. 9 The simulation of the changes of the O V and O VI with compression. solid lines: before compression; dot lines: comsidering the changes of $n_e(r)$ and $T_e(r)$ by compression but without the changes of transport coefficients, dashed lines: not only considering the changes of $n_e(r)$ and $T_e(r)$, but also the changes of transport coefficients.

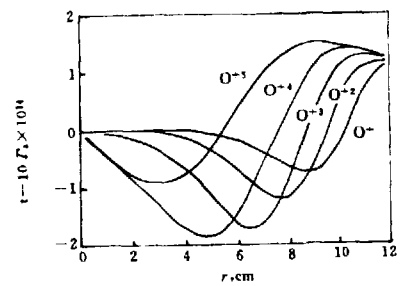

Fig. 10 The simulated transport fluxes of $O^+ \sim O^+5$.

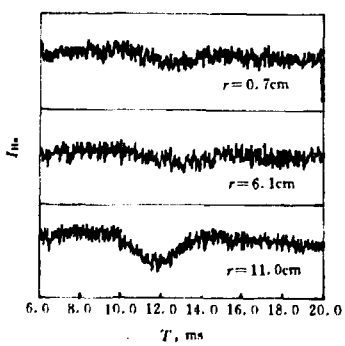

Fig. 11 The multichannel H_α signals in magnetic compression (compression starting at about $t=10.0$ms).

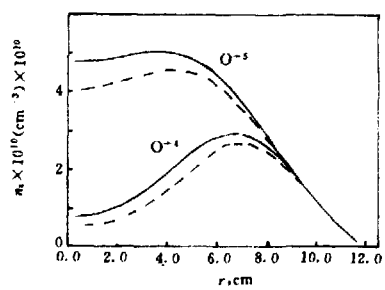

Fig. 12 The comparison of the density profiles of O^+4 and O^+5 in the two cases with 20% defference of $T_e(r)$, solid line: $T_e(O)=185$eV; dotted line: $T_e(O)=155$eV.

HT-6B 托卡马克杂质输运
原子能出版社出版
（北京 2108 信箱）
中国核情报中心排版
北京市海淀区三环快速印刷厂印刷
☆
开本 787×1092 1/16 · 印张 1 · 字数 12 千字
1992 年 6 月北京第一版 · 1992 年 6 月北京第一次印刷
ISBN 7-5022-0717-1
TL · 445

CHINA NUCLEAR SCIENCE & TECHNOLOGY REPORT

ISBN 7-5022-0717-1
TL • 445

P.O.Box 2103
Beijing, China

China Nuclear Information Centre